Supplementary Information

Controlled synthesis of $Sb_2(S_{1-x}Se_x)_3$ ($0 \leq x \leq 1$) Solid Solution and the Effect of Composition Variation on Eletrocatalytic Energy Conversion and Storage

Malik Dilshad Khan,[1]* Saif Ullah Awan,[2] Camila Zequine,[3] Chunyang Zhang,[3] Ram K. Gupta,[3] and Neerish Revaprasadu[1]*

[1]Department of Chemistry, University of Zululand, Private Bag X1001, KwaDlangezwa 3886, South Africa.

[2]Department of Electrical Engineering, NUST College of Electrical and Mechanical Engineering, National University of Sciences and Technology (NUST) Islamabad 44000, Pakistan.

[3]Department of Chemistry, Pittsburg State University, Pittsburg, KS 66762, USA.

Corresponding Authors

*Email: RevaprasaduN@unizulu.ac.za
*Email: malikdilshad@hotmail.com

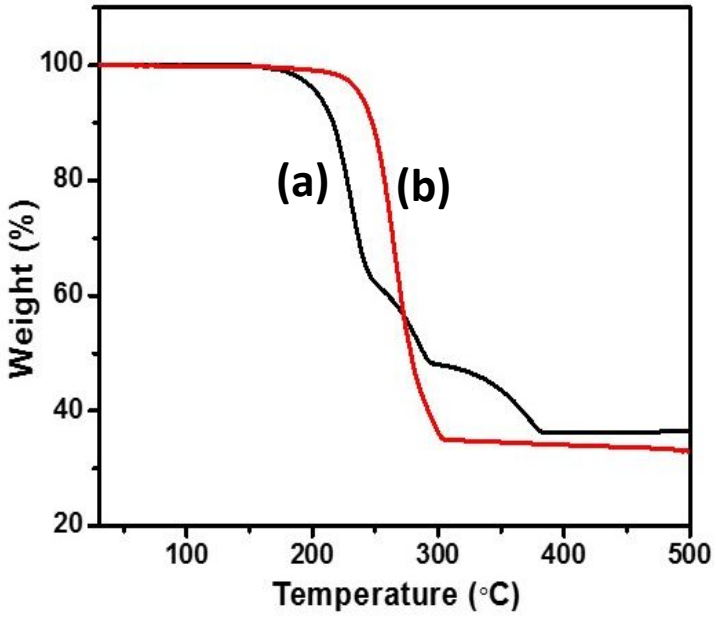

Figure S1. Thermogravimetric analysis of (a) complex (1) and (b) complex (2).

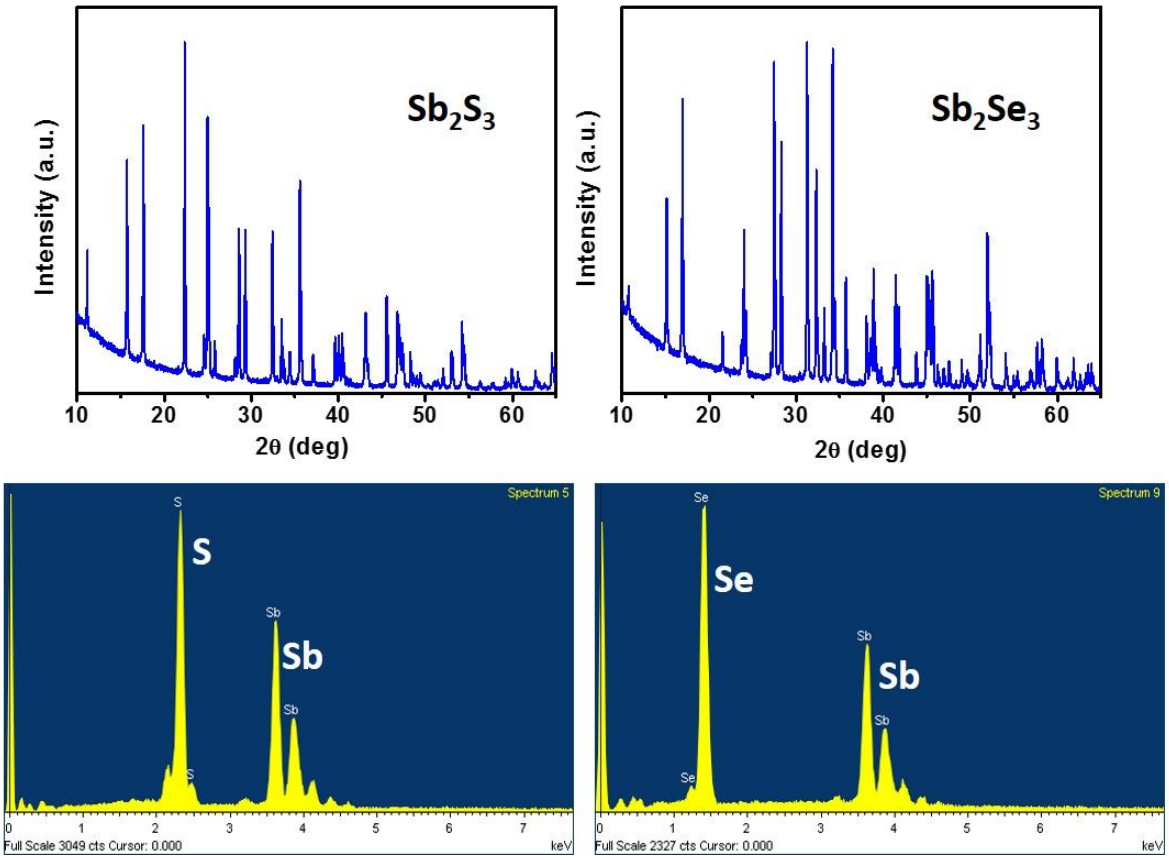

Figure S2. Diffraction pattern of Sb_2S_3 and Sb_2Se_3, obtained from decomposition of *tris*(thiobenzoato)Sb(III) and *tris*(selenobenzoato)Sb(III), respectively.

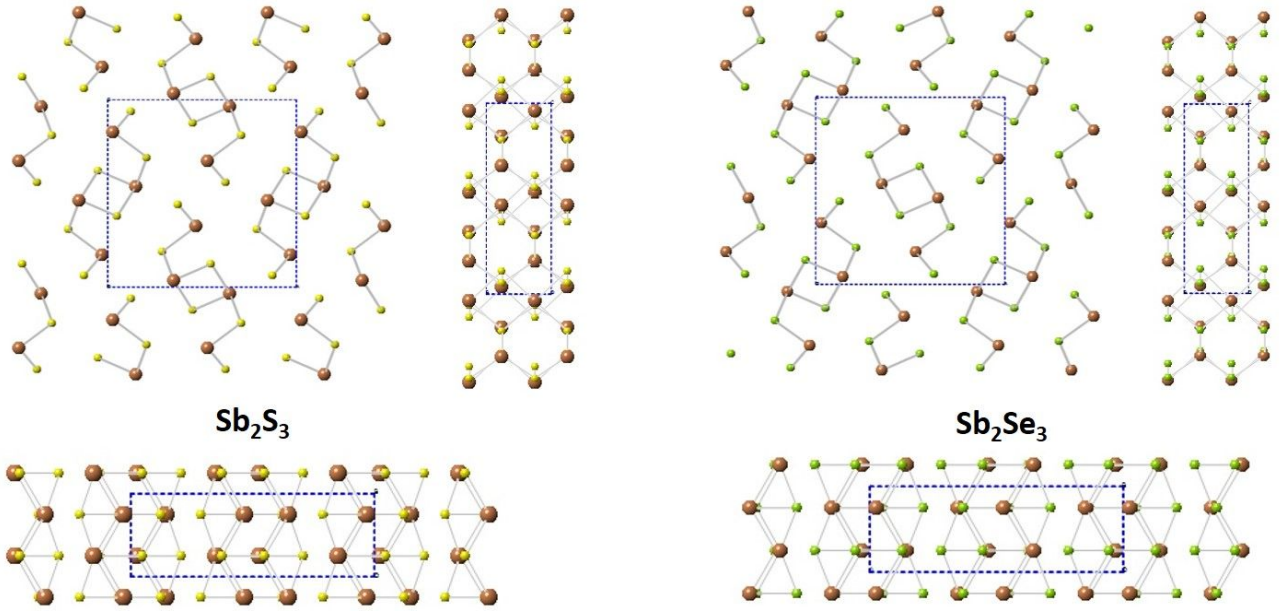

Figure S3. Crystal structure of Sb_2S_3 and Sb_2Se_3 viewed along different axis.

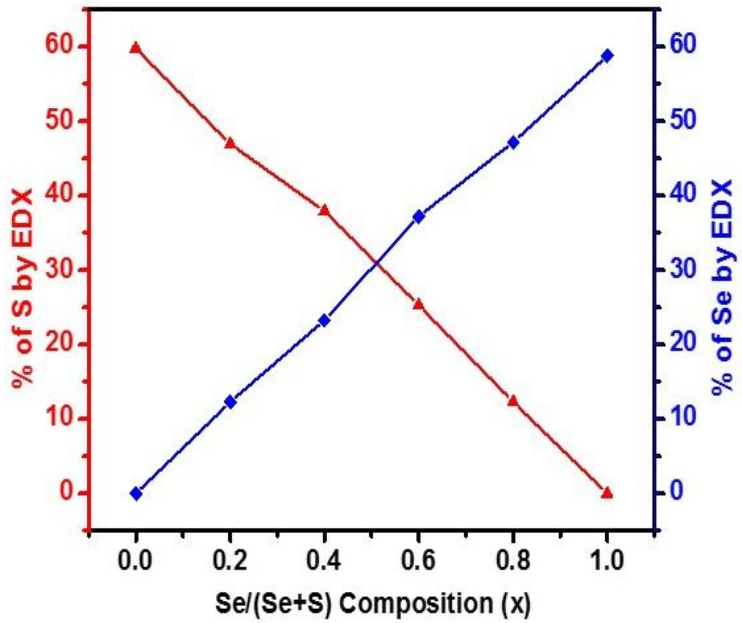

Figure S4. Plot showing change in concentration of Selenium and Sulfur content against Se/(Se+S) composition.

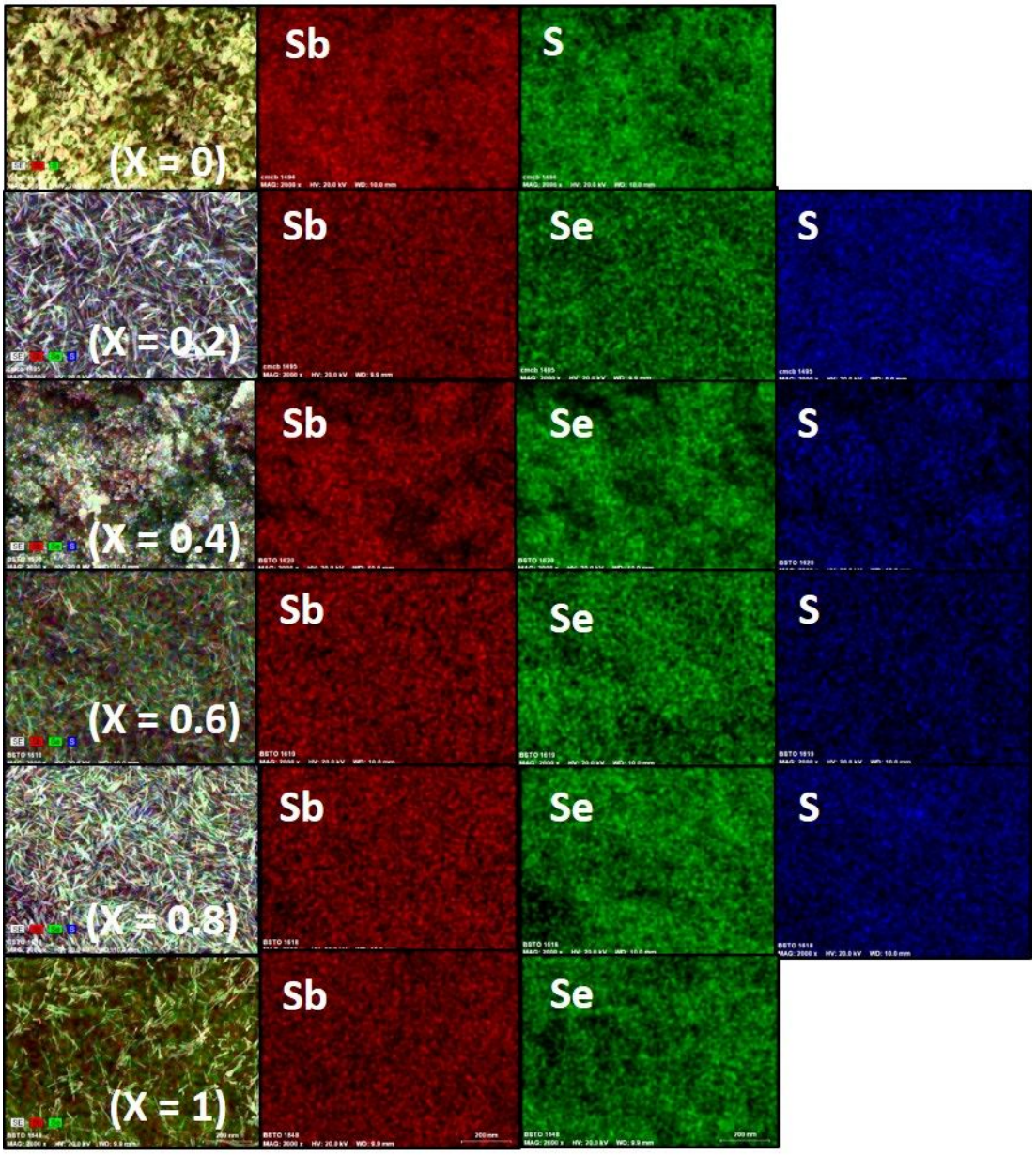

Figure S5. Elemental mapping of samples with different selenium concentration, showing uniform distribution of antimony, sulfur and selenium.

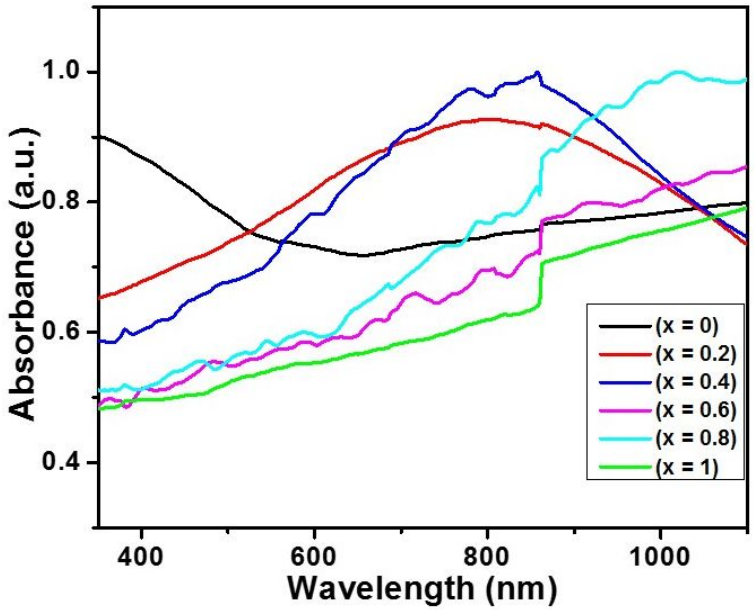

Figure S6. UV-Vis-NIR spectroscopic analysis of the binary and ternary nanomaterials with different stoichiometry of $Sb_2(S_{1-x}Se_x)_3$ (where $0 \leq x \leq 1$), indicating shift in absorption peaks.

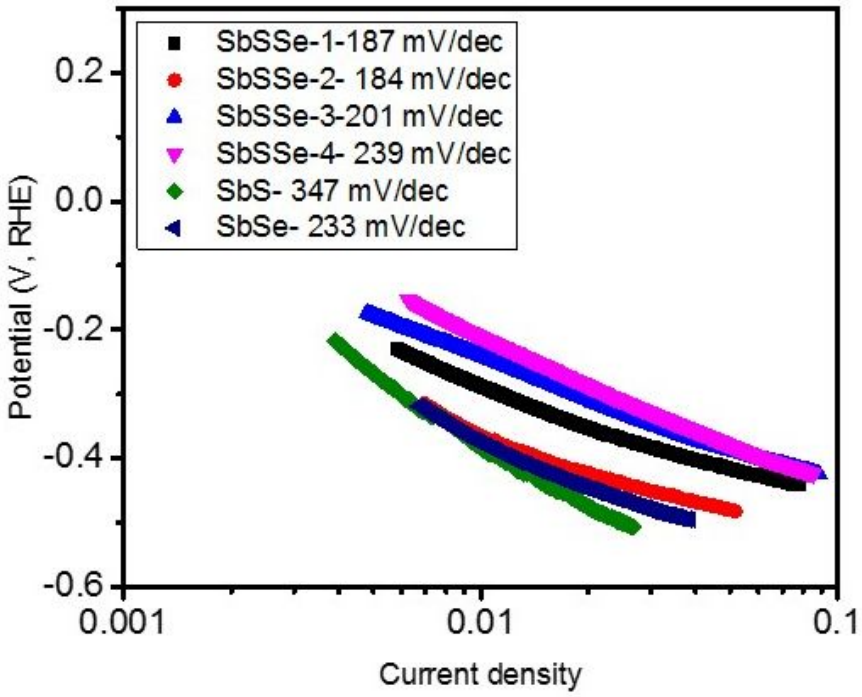

Figure S7. Tafel slopes of all $Sb_2(S_{1-x}Se_x)_3$ (where $0 \leq x \leq 1$), samples.

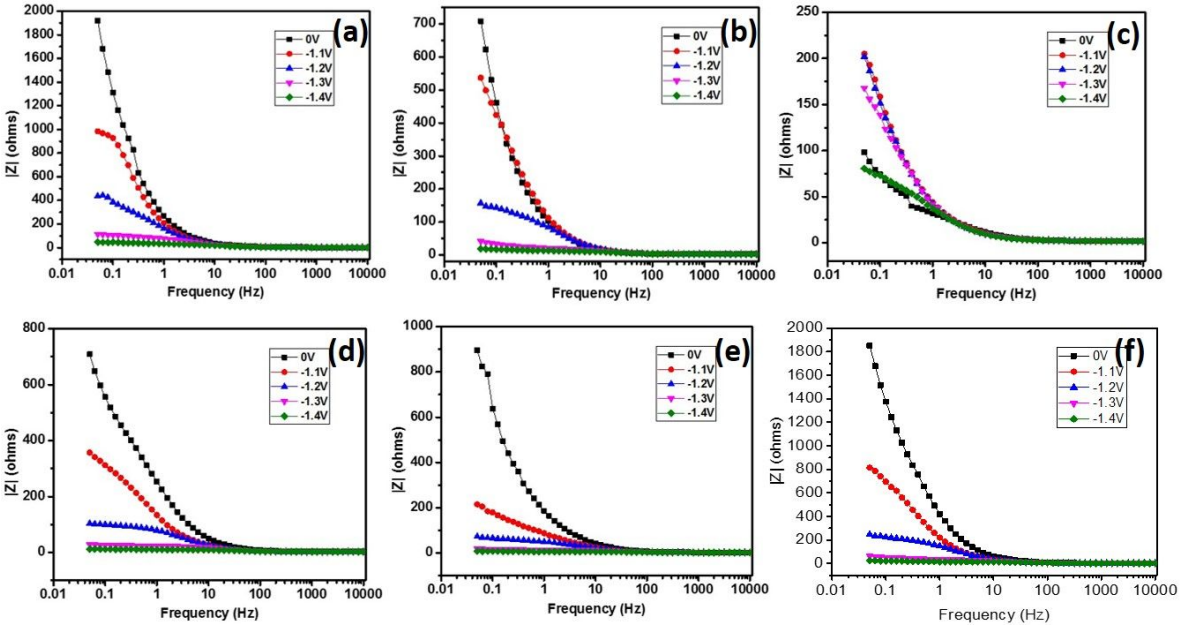

Figure S8. |Z| vs. frequency plots for (a)SbS, (b) SbSSe-1, (c) SbSSe-2, (d) SbSSe-3, (e) SbSSe-4 and (f) SbSe samples.